Eur. Phys. J. C (2025) 85:372
https://doi.org/10.1140/epjc/s10052-025-14102-3

THE EUROPEAN PHYSICAL JOURNAL C

Regular Article - Theoretical Physics

Nonmetricity-based hybrid self-gravitating compact stars with embedded class-one symmetry

Naveed Iqbal[1,a], **S. Khan**[2,b], **Mohammad Alshammari**[1,c], **Wael W. Mohammed**[1,d], **M. Ilyas**[3,e]

[1] Department of Mathematics, College of Science, University of Haíl, Haíl 2440, Saudi Arabia
[2] University of Agriculture Faisalabad, Constituent College, Toba Tek Singh 36050, Pakistan
[3] Institute of Physics, Gomal University, Dera Ismail Khan, KP 29220, Pakistan

Received: 3 February 2025 / Accepted: 19 March 2025

Abstract This work aims to explore the novel characteristics of a static hybrid transitional star with a spherical distribution of relativistic matter under the embedded class one metric framework. This theoretical stellar model is derived using the nonmetricity-inspired $f(\mathbb{Q})$ gravity, featuring a core-crust structure: a strange matter core embedded in a normal matter crust. Our model incorporates pressure anisotropy as an intrinsic characteristic of highly compact strange stars, a feature expected to arise in the super-dense regime. The equation of state, in its basic form, using the MIT bag model is employed to represent correlation between pressure and density in quark matter inside the star's core. The development of this model involves selecting the temporal gravitational potential based on the Tolman–Kuchowicz ansatz, while the radial gravitational potential is determined using the Class One embedding formalism. We employed both analytical and graphical methods to assess the robustness and equilibrium of the presented stellar solution. We provide an in-depth description of the astrophysical features of the model and show that they fulfill regularity requirements. A key finding of this investigation is the absence of a core singularity within the anisotropic stellar formation. The solution matches the properties of the observed self-gravitating pulsar objects: SAX J1804.4-3658 (SS1), EXO1745-248, 4U1820-30, 4U1608-52, PSR J0740+6620, PSR J0030+0451, Cen X-4, and SAX J1804.4-3658 (SS2).

1 Introduction

Hybrid neutron stars represent an intriguing class of dense-matter stellar configurations that enhance our understanding of both the peculiar phases of matter proposed by high-energy physics and standard neutron star models [1,2]. These strange stellar formations are believed to feature a dense core containing deconfined quark matter (QM) or other exotic states, surrounded by an outer region of nuclear matter composed of baryons and neutrons. Their research serves as a searchlight for astrophysical and cosmic processes and offers new perspectives on the fundamental physics of highly dense matter content. These supernova remnants, like regular neutron stars, have a crust composed of ions, electrons, and neutron-rich nuclei. However, their cores are believed to contain deconfined QM or other exotic phases, such as strange QM or states characterized by color superconductivity. It is hypothesized that phase shift, governed by the MIT bag model [3], drives the shift from hadronic matter to QM, resulting in a specialized EoS that integrates quark and nuclear physics. The observable macroscopic characteristics of the stellar configuration, including its mass-radius relationship, susceptibility to tidal deformation, and long-term thermal behavior, are significantly influenced by the presence of a mixed-phase core. Gravitational wave signals from neutron star mergers and surveys of large pulsars can provide significant constraints on the presence and properties of hybrid QM stars [4]. Furthermore, these strange configurations are crucial for understanding astrophysical events like cataclysmic stellar explosions, high-energy bursts, and the cooling behavior of confined cosmic objects. Through multi-messenger astrophysics, studying hybrid neutron stars provides a unique laboratory for expanding our insight into

[a] e-mail: n.iqbal@uoh.edu.sa
[b] e-mail: suraj.pu.edu.pk@gmail.com (corresponding author)
[c] e-mail: dar.alshammari@uoh.edu.sa
[d] e-mail: w.mohammed@uoh.edu.sa
[e] e-mail: m.ilyas@gu.edu.pk

Published online: 02 April 2025

quantum chromodynamics, the core of strong interactions, and the expanding cosmos [5].

Recent advances in cosmology and astrophysical physics have placed significant focus on the spatial organization of the rapid cosmic acceleration [6–8]. New developments in this cosmic epoch have revealed new ways to understand the basic and empirical changes that are causing the galaxy to evolve so rapidly. This rapid expansion is implicitly supported by a number of findings, including strong evidence from extreme redshift supernova observations [9], large-scale structures [10], and fluctuations in Cosmic Microwave Background Radiation [11]. Our universe undergoing rapid expansion due to an unknown phenomenon called dark energy, which exerts a strong negative pressure. As a result, modifications to traditional gravitational models are necessary to evaluate the phenomenon of rapid cosmic acceleration. These observations encourage the possibility of extended or modified gravitational frameworks that can accurately represent scenarios where general relativity (GR) produces insufficient results. Cosmologists are actively exploring alternative gravitational theories to tackle the constraints of GR in explaining the exponential cosmic acceleration. Prominent examples of non-standard gravity models, such as $f(R)$, $f(G)$, $f(R,T)$, $f(G,T)$, and $f(R,T^2)$ [12–24]. These theories offer several astrophysical and cosmological perspectives and conclusions that help address the enigmas surrounding the phenomenon of rapid galactic expansion. Astrophysical evidence provides a vital testing ground for higher-curvature models of gravity. Strong-field scenarios, such as those near black holes or neutron stars, are crucial for distinguishing between GR and its possible extensions, as these theories often coincide with GR in weak-field regimes. Since dense-matter relativistic configurations, such as neutron stars, exist in intense gravitational fields, these stellar structures can be examined to determine whether the proposed modified gravity theory deviates from GR. Additionally, multiple lines of evidence strongly indicate the presence of dark matter. Extended gravitational models can also be employed to explain these phenomena without integrating novel matter fields or non-standard energy sources. The complex mechanism of dense-matter compositions has been explored by several researchers using higher-curvature ingredients within different backgrounds [25–30].

Following the development of GR, the majority of gravity models are developed inside a geometrical foundation that excludes non-metricity and torsion [31–34]. Alternatively, gravitational models can be constructed using scalars related to non-metricity ($\mathbb{Q}$) and torsion (T). Although the actions $\int d^4x\sqrt{-g}\ \mathbb{Q}$ and $\int d^4x\sqrt{-g}\ T$ are equivalent to GR in the context of flat spacetime, their generalizations, expressed through $f(T)$ [35–37] and $f(\mathbb{Q})$ [38–40], can be classified as modifications to classical GR. The $f(\mathbb{Q})$ gravity model has been used across multiple fields, including large-scale structure composition [41], relativistic modified Newtonian dynamics [42,43], bouncing cosmologies [44–46], and quantum cosmology [47,48]. Multiple research works have focused on understanding the implications of $f(\mathbb{Q})$ gravity in astrophysical and cosmic scenarios. Wang et al. [49] developed spherically symmetric stellar configurations featuring anisotropic fluid by employing the $f(\mathbb{Q})$ gravity. They pointed out that the assumption of coincident gauge results into rigorous constraints on the function $f(\mathbb{Q})$. Lin and Zhai [50] examined the influence of non-metricity-based $f(\mathbb{Q})$ gravity on the static, dense-matter spherical configurations by constructing the internal and external stellar models. They showed that the coupling of polytropic EoS with the quadratic function $f(\mathbb{Q}) = \mathbb{Q} + \alpha\mathbb{Q}$, where $\alpha < 0$, enables the formulation of more massive stellar configurations in the enteral case. However, the external solutions coincides with the classical GR solutions for any analytical form of $f(\mathbb{Q})$ model.

Several investigations into understanding the effects of non-metricity on the physical features of DE stars, strange stars, and hybrid stellar configurations have been conducted in recent years. By employing the second-order formulation of $f(\mathbb{Q})$ model, Bhar et al. [51] examined an emerging family of DE stars with static and spherically symmetric relativistic matter configurations. This analysis reveals a significant finding: the radii corresponding to the maximum masses exhibit an increasing trend as the model parameter decreases. Bhar and Pretel [52] explored the complex composition of DE stars and hybrid stars using non-metricity-based linear analytical formulation of $f(\mathbb{Q})$ gravity. Bhar and Rahaman [53] developed an anisotropic DE stellar model with a distinctive five-zone density configuration by employing classical GR. The physical acceptability of the proposed stellar solution was analyzed by applying small radial perturbations. Maurya et al. [54] analyzed the role of electric charge on the configurations of anisotropic gravitationally confined compact solutions through the mechanism of linear $f(\mathbb{Q})$ gravity. The stability and regularity of the proposed model were examined through stringent physical constraints.

For describing the matter distribution of dense-matter relativistic formations, local isotropy is one of the most frequently employed assumptions when modeling a particular stellar object. This Pascalian nature of fluids, characterized by the equality of principal stresses, is well-supported by extensive observational evidence. However, recent decades have witnessed a surge in theoretical studies suggesting that local anisotropy may arise within specific density ranges, deviating from the Pascalian behavior [55–61]. Anisotropic pressure is a primary tool for identifying the formation and characteristics of relativistic matter under extreme conditions, particularly in astrophysical scenarios involving self-gravitating configurations such as stars, galaxies, and compact structures (e.g., neutron stars and quark stars) [62–64]. Anisotropy refers to the phenomenon where the fluid pres-

sure is separated into radial (P_r) and tangential (P_t?) contributions, in contrast to isotropic systems characterized by uniform pressure in all directions. Anisotropic pressure in astrophysical models of stellar interiors can arise from various phenomena, including rotation, magnetic fields, viscosity, the geometry of π^- modes [65], and exotic matter. The stability, structure, and evolution of such condensed matter objects can be significantly influenced by these directional pressure fluctuations. Recognizing the complexity of stellar formations, models now often incorporate anisotropic matter, including scenarios such as the presence of type P superfluids, phase transitions, solid cores, or boson stars [66,67]. Local anisotropy in low-density astrophysical configurations, such as spherical galactic structures, can be attributed to the seminal contributions of Jeans [68]. This anisotropy arises directly from non-uniform velocity distributions within these systems. Ruderman [69] theoretically proposed that anisotropy in dense-matter relativistic systems could arise as a consequence of extremely high densities, i.e., on the order of 10^{15}g/cm^3, a characteristic feature of astrophysical models.

Anisotropy can potentially impact the stability of compact stars, causing deviations from conventional models of stellar evolution or increasing the likelihood of collapse in specific scenarios [70,71]. In cosmological simulations, anisotropy is critical, particularly in understanding different phases of cosmic evolution or modified stellar models. The presence of anisotropy in these models can lead to deviations from conventional cosmological models, potentially offering alternative explanations for phenomena such as DE, the acceleration of cosmic expansion, or the formation of cosmic structures, differing from predictions of isotropic models. Furthermore, in the context of extremely dense-matter configurations, such as black holes and other gravitationally confined systems, anisotropic models provide a more comprehensive framework for understanding the underlying gravitational field. These models account for possible deviations in pressure and density, particularly within strong gravitational regimes where modifications to GR may be required. Additionally, anisotropy facilitates the representation of different phases of matter, such as those found within stars or near black holes, offering new insights into how matter behaves under extreme conditions.

The following layout is used to present our analysis. Section 2 provides the underlying framework of the Embedding Class One symmetry within the framework of spherically symmetric line element. Section 3 presents the relativistic dynamics of the $f(\mathbb{Q})$ model of gravitational interactions. In Sect. 4, we develop non-metricity-based self-gravitating hybrid star models, regulated by normal matter and quark matter, within the background of the coincident gauge. Structural features ensuring the physical viability of the presented anisotropic hybrid configuration, such as energy bounds, hydrostatic equilibrium criteria, and stability analysis through different techniques, are discussed in Sect. 5. Some additional features, including the mass function, gravitational characteristics and surface redshift of the presented solution, are examined in Sect. 6. In Sect. 7, we present the concluding remarks pertinent to this study.

2 Embedding class one metric: a spherically symmetric scheme

A spacetime is categorized as Class One if it can be geometrically embedded within a five-dimensional pseudo-Euclidean space. This is achievable only if a symmetric tensor, called the second fundamental form ($K_{\mu\nu}$), fulfills the equations

$$R_{\mu\nu\sigma\rho} = \varepsilon(K_{\mu\sigma}K_{\nu\rho} - K_{\mu\rho}K_{\nu\sigma}), \tag{1}$$

$$\nabla_\sigma K_{\mu\nu} = \nabla_\nu K_{\mu\sigma}. \tag{2}$$

Here, the mathematical quantity $R_{\mu\nu\sigma\rho}$ signifies the Riemann tensor, and $\varepsilon = \pm 1$ (depending on whether the normal to the manifold is time-like "−" or space-like "+"). In this work, we adopt a static metric ansatz to describe the geometry of the gravitational field surrounding a spherical stellar configuration, defined as

$$ds^2 = e^a dt^2 - e^b dr^2 - r^2\left(d\theta^2 - \sin^2\theta d\phi^2\right), \tag{3}$$

where due to imposed symmetry $a = a(r)$ and $b = b(r)$ are exclusively functions of r. Thus, the only non-zero terms of $K_{\mu\nu}$, corresponding to the metric ansatz (3), are: K_{00}, $K_{01} = K_{10}$, K_{11} and $K_{22} = K_{33}\sin^2\theta$. Upon plugging these components in Eq. (1), we obtain the following result [72]

$$R_{1010} = \frac{R_{1212}R_{3030} + R_{1220}R_{1330}}{R_{2323}}, \tag{4}$$

with $R_{2323} \neq 0$ [73], this defines the embedding Class One metric. Then, the combination of Eqs. (3) and (4) produces

$$2\frac{a''}{a'} + a' = \frac{b'e^b}{e^b - 1}, \tag{5}$$

where $e^b \neq 0$. The integration of Eq.(5) provides

$$e^b = 1 + b'^2 S e^a. \tag{6}$$

We consider the temporal gravitational potential using the well-defined Tolman–Kuchowicz metric (TK-metric, hereafter) ansatz, expressed as

$$a(r) = Ar^2 + 2\ln B. \tag{7}$$

Here, B is a dimensionless constant, whereas A is a constant with dimensions of [length^{-2}]. The ability of the TK-metric to provide analytical solutions to the equations of motion within the dynamics of GR and modified gravitational formalism, under spherically symmetric and static scenarios, makes it an important tool for modeling stellar configurations [74,75]. Understanding the complex characteristics of gravitationally bound compact formations, such as neutron stars and quark stars, is facilitated by its well-defined and theoretically tractable metric functions. Additionally, it supports a wide variety of EoSs utilized in the simulation of gravitationally bound formations. The metric ansatz (7) has been employed by numerous researchers to obtain solutions to stellar structure equations for self-gravitational stellar configurations. Bhar [76] developed a model of a self-gravitating compact configuration fueled by a dark energy EoS using the TK-metric. Furthermore, the author explored the astrophysical features of dark energy gravitational stars through modified gravity [76]. The TK-metric serves as an essential framework for investigating how relativistic gravity, matter composition, and spacetime curvature affect compact star configurations. Its adaptability and stability make it crucial to relativistic astrophysics and compact star models.

Next, by using Eq. (7) in Eq. (6), we get the radial gravitational potentials as

$$b(r) = \ln\left(1 + 4SA^2B^2r^2e^{Ar^2}\right). \tag{8}$$

3 Relativistic dynamics of $f(\mathbb{Q})$ gravity

The action of $f(\mathbb{Q})$ gravity, which generalizes the symmetric teleparallel formalism by substituting the non-metricity scalar $\mathbb{Q}$ with a generic functional form $f(\mathbb{Q})$, is defined as [77]

$$S = \frac{1}{2}\int d^4x\sqrt{-g}f(\mathbb{Q}) + S_{\text{matter}}. \tag{9}$$

In this theory, both the metric tensor $g_{\mu\nu}$ and the affine connection $\Gamma^{\sigma}_{\ \mu\nu}$ act as fundamental variables, making it a metric-affine theory. Therefore, to obtain the field equations corresponding to this gravity model, we must perform variations concerning both $g_{\mu\nu}$ and $\Gamma^{\sigma}_{\ \mu\nu}$ independently. We define the torsion and non-metricity tensors as

$$T^{\sigma}_{\ \mu\nu} := \Gamma^{\sigma}_{\ \mu\nu} - \Gamma^{\sigma}_{\ \nu\mu}, \tag{10}$$

$$\mathbb{Q}_{\rho\mu\nu} := \nabla_\rho g_{\mu\nu} = \partial_\rho g_{\mu\nu} - \Gamma^{\eta}_{\ \rho\mu}g_{\sigma\nu} - \Gamma^{\sigma}_{\ \rho\nu}g_{\mu\sigma}. \tag{11}$$

Under these conditions, we have

$$\Gamma^{\sigma}_{\ \mu\nu} = \left\{^{\sigma}_{\ \mu\nu}\right\} + \mathbb{S}^{\sigma}_{\ \mu\nu}, \tag{12}$$

where $\left\{^{\sigma}_{\ \mu\nu}\right\}$ denotes the Levi-Civita connection

$$\left\{^{\sigma}_{\ \mu\nu}\right\} = \frac{1}{2}g^{\sigma\rho}\left(\partial_\mu g_{\rho\nu} + \partial_\nu g_{\rho\mu} - \partial_\rho g_{\mu\nu}\right), \tag{13}$$

and

$$\mathbb{S}_{\sigma\mu\nu} = -\frac{1}{2}(T_{\mu\nu\sigma} + T_{\nu\mu\sigma} - T_{\sigma\mu\nu}) - \frac{1}{2}(\mathbb{Q}_{\mu\nu\sigma} + \mathbb{Q}_{\nu\mu\sigma} - \mathbb{Q}_{\sigma\mu\nu}), \tag{14}$$

is referred to as the distortion tensor. Let us now introduce the following non-metricity conjugate

$$P^{\rho\mu\nu} = -\frac{1}{4}\mathbb{Q}^{\rho\mu\nu} + \frac{1}{2}\mathbb{Q}^{(\mu\nu)\rho} + \frac{1}{4}(\mathbb{Q}^{\rho} - \widetilde{\mathbb{Q}}^{\rho})g^{\mu\nu} - \frac{1}{4}g^{\rho(\mu}\mathbb{Q}^{\nu)}. \tag{15}$$

Here, the terms $\mathbb{Q}_\rho$ and $\widetilde{\mathbb{Q}}_\rho$ represent two independent traces associated with $\mathbb{Q}_{\rho\mu\nu}$

$$\mathbb{Q}_\rho = g^{\eta\sigma}\mathbb{Q}_{\rho\eta\sigma}, \quad \widetilde{\mathbb{Q}}_\rho = g^{\eta\sigma}\mathbb{Q}_{\eta\rho\sigma}, \tag{16}$$

Consequently, the non-metricity scalar can be defined by the following expression

$$\mathbb{Q} = -\mathbb{Q}_{\rho\mu\nu}P^{\rho\mu\nu}. \tag{17}$$

$$\mathcal{X}_{\mu\nu} \equiv \frac{2}{\sqrt{-g}}\nabla_\rho\left(\sqrt{-g}f_{\mathbb{Q}}P^{\rho}_{\ \mu\nu}\right) - \frac{1}{2}g_{\mu\nu}f + \left(P_{\mu\sigma\eta}\mathbb{Q}_{\nu}^{\ \rho\eta} - 2P_{\rho\eta\mu}\mathbb{Q}^{\rho\eta}_{\ \ \nu}\right)f_{\mathbb{Q}} = 8\pi\overset{\circ}{T}_{\mu\nu} \tag{18}$$

Here, $f_{\mathbb{Q}} \equiv \partial_{\mathbb{Q}}f(\mathbb{Q})$ and for notational convenience, the equations of motion of the metric are represented by $\mathcal{X}_{\mu\nu}$. Being a metric-affine theory, the solutions to $f(\mathbb{Q})$ theory should satisfy the zero-curvature and zero-torsion conditions by incorporating both metric and symmetric teleparallel GR covariant derivatives. Since GR is merely a metric-dependent theory, we believe this result illustrates that there are more possibilities to develop solutions incorporating additional gravitational effects in modified symmetric teleparallel GR theories [78,79]. Furthermore, the stress-energy tensor (SET) for the stellar system is described

$$\overset{\circ}{T}_{\mu\nu} \equiv \frac{2}{\sqrt{-g}}\frac{\delta(\sqrt{-g}\mathscr{L}_m)}{\delta g^{\mu\nu}}. \tag{19}$$

Next, the variation of the gravitational action (9) concerning the affine connection provides the following stellar equations

$$\nabla_\mu\nabla_\nu(\sqrt{-g}f_{\mathbb{Q}}P^{\mu\nu}_{\ \ \alpha}) = 0. \tag{20}$$

The field equations associated with $f(\mathbb{Q})$ gravity ensure the conservation of the SET and reduce to GR in the limit $f(\mathbb{Q}) \to \mathbb{Q}$.

As discussed in [80], one can consider a particular coordinate system $\{y^\mu\}$, where the affine connection $\Gamma^\lambda_{\ \mu\nu}(y^\lambda)$ is zero. This is defined as the coincident gauge [78]. Transforming to any other coordinate system $\{x^\mu\}$ results in the following form for the affine connection

$$\Gamma^\lambda_{\ \mu\nu}(x^\mu) = \left(\frac{\partial x^\lambda}{\partial y^\varepsilon}\right)\partial_\mu\partial_\nu y^\varepsilon. \tag{21}$$

Consequently, the non-metricity tensor simplifies to

$$\mathbb{Q}_{\rho\mu\nu} = \partial_\rho g_{\mu\nu}. \tag{22}$$

We assume a time-independent metric in curvature coordinates $(x^0, x^1, x^2, x^3) \equiv (t, r, \theta, \phi)$, defined as

$$ds^2_- = e^{a(r)}dt^2 - e^{b(r)}dr^2 - r^2\left(d\theta^2 + \sin^2\theta d\phi^2\right). \tag{23}$$

The expression for the non-metricity scalar of the above-mentioned metric reads

$$\mathbb{Q} = -2e^{-b}\left(\frac{a'}{r} + \frac{1}{r^2}\right), \tag{24}$$

The SET characterizing the distribution of hybrid matter can be defined by the following decomposed relation

$$\overset{\circ}{T}_{\mu\nu} = T_{\mu\nu} + \widetilde{T}_{\mu\nu}, \tag{25}$$

where $T_{\mu\nu}$ and $\widetilde{T}_{\mu\nu}$ denote the contributions of normal matter and the quark matter, respectively. The matrix form of the SET (25) can be represented as

$$\begin{aligned}\overset{\circ}{T}^\mu_{\ \nu} &= \begin{pmatrix} \overset{\circ}{\sigma} & 0 & 0 & 0 \\ 0 & -\overset{\circ}{P}_r & 0 & 0 \\ 0 & 0 & -\overset{\circ}{P}_t & 0 \\ 0 & 0 & 0 & -\overset{\circ}{P}_t \end{pmatrix} \Rightarrow \overset{\circ}{T}^\mu_{\ \nu} \\ &= \begin{pmatrix} \sigma+\sigma^q & 0 & 0 & 0 \\ 0 & -(P_r+P_r^q) & 0 & 0 \\ 0 & 0 & -(P_t+P_t^q) & 0 \\ 0 & 0 & 0 & -(P_t+P_t^q) \end{pmatrix},\end{aligned} \tag{26}$$

such that $\overset{\circ}{P}_r \neq \overset{\circ}{P}_t$. The non-zero components of SET are then $\overset{\circ}{T}^0_{\ 0} = \overset{\circ}{\sigma}$, $\overset{\circ}{T}^1_{\ 1} = -\overset{\circ}{P}_r$, and $\overset{\circ}{T}^2_{\ 2} = \overset{\circ}{T}^3_{\ 3} = -\overset{\circ}{P}_t$. In addition, σ^q, P_r^q, P_t^q represent the density and the pressure components corresponding to the quark matter. Finally, the stellar model for the linear $f(\mathbb{Q})$ model is characterized by the following differential equations

$$\mathcal{X}_{00} = 8\pi\overset{\circ}{T}_{00}: \ \frac{f}{2} - f_\mathbb{Q}\left\{\mathbb{Q} + \frac{1}{r^2} + \frac{e^{-b}}{r}(a'+b')\right\} = -8\pi\overset{\circ}{\sigma}, \tag{27}$$

$$\mathcal{X}_{11} = 8\pi\overset{\circ}{T}_{11}: \ \frac{f}{2} - f_\mathbb{Q}\left(\mathbb{Q} + \frac{1}{r^2}\right) = 8\pi\overset{\circ}{P}_r, \tag{28}$$

$$\begin{aligned}\mathcal{X}_{22} = 8\pi\overset{\circ}{T}_{22}: \ &\frac{f}{2} - f_\mathbb{Q}\left\{\frac{\mathbb{Q}}{2} - e^{-b}\left[\frac{a''}{2} + \left(\frac{a'}{4} + \frac{1}{2r}\right)(a'-b')\right]\right\} \\ &= 8\pi\overset{\circ}{P}_t,\end{aligned} \tag{29}$$

$$\mathcal{X}_{12} = 8\pi\overset{\circ}{T}_{21}: \ \frac{\mathbb{Q}'}{2}\cot\theta f_{\mathbb{Q}\mathbb{Q}} = 0. \tag{30}$$

That is, assuming a vanishing affine connection in the spherically symmetric coordinate system and requiring vacuum solutions for $f(\mathbb{Q})$ theory ($\mathcal{X}_{\mu\nu} = 0$), the non-diagonal terms of the equations of motion yield the result $f_{\mathbb{Q}\mathbb{Q}} = 0$. This implies that $f(\mathbb{Q})$ must be linear. Nonlinear alternatives for $f(\mathbb{Q})$, such as $f(\mathbb{Q}) = \mathbb{Q}^2$, lead to inconsistencies in the field equations and their solutions. Thus, nonlinear functional forms of $f(\mathbb{Q})$ are not favorable for producing viable solutions to the field equations.

4 Modeling hybrid stars within $f(\mathbb{Q})$ gravity

For developing viable and realistic stellar solutions that characterize self-gravitating stars, an appropriate formulation of the function $f(\mathbb{Q})$ is a key ingredient. Concerning this, Wang et al. [49] suggested physically realistic static, self-gravitating solutions by restricting the formulation of $f(\mathbb{Q})$ to the linear case. The resulting solutions correspond to the Schwarzschild (Anti-) de Sitter model. Therefore, to examine physically feasible star models, we select a linear formulation of $f(\mathbb{Q})$, which is given by [51]

$$f(\mathbb{Q}) = \beta + \alpha\mathbb{Q}. \tag{31}$$

Here, α and β are constants. Choosing $\alpha = 1$ and $\beta = 0$ reproduces the results of classical GR.

To solve the stellar equations using linear $f(\mathbb{Q})$ formulation, we assume a standard EoS for strange matter: the MIT bag model [81,82]. An EoS of this form has been extensively purposed for developing realistic modeling of strange matter stellar configurations. This EoS defines the correspondence between matter density and pressure through the bag constant B_g as follows

$$P^q = \frac{1}{3}(\sigma^q - 4B_g). \tag{32}$$

For the usual matter distribution, we assume the following proportional relationship

$$P_r \propto \sigma \quad \Rightarrow \quad P_r = m\sigma, \tag{33}$$

where $m \in (0, 1)$ such that $m \neq \frac{1}{3}$, is an EoS parameter.

Then, using the gravitational potentials (7) and (8), we obtain the following set of stellar equations

$$8\pi(\sigma + \sigma^q) = \frac{16\alpha A^3 B^2 S r^2 e^{Ar^2} - \beta + 8A^2 B^2 S e^{Ar^2}\left(3\alpha - \beta r^2\right) - 16A^4 B^4 S^2 r^2 e^{2Ar^2}\left(-2\alpha + \beta r^2\right)}{2\left(1 + 4A^2 B^2 S r^2 e^{Ar^2}\right)^2}, \tag{34}$$

$$8\pi(P_r + P^q) = \frac{4\alpha A + \beta - 4A^2 B^2 S e^{Ar^2}\left(2\alpha - \beta r^2\right)}{2 + 8A^2 B^2 S r^2 e^{Ar^2}}, \tag{35}$$

$$8\pi(P_t + P^q) = \frac{2\alpha A + \beta + 16\beta A^4 B^4 S^2 r^2 e^{2Ar^2} + A^2\left(-4\alpha B^2 S e^{Ar^2} + r^2\left(\beta + 8\beta B^2 S e^{Ar^2}\right)\right)}{2\left(1 + 4A^2 B^2 S r^2 e^{Ar^2}\right)^2}. \tag{36}$$

Thus, the values of the thermodynamical quantities corresponding to the self-gravitating hybrid star model, under the gravitational potentials (7) and (8), are defined as

$$\begin{aligned}\sigma = &\Big[16\pi B_g\left(1 + 4A^2 B^2 S r^2 e^{Ar^2}\right)^2 + 3\alpha A \\ &+ 8\alpha A^3 B^2 S r^2 e^{Ar^2} + \beta - 4A^2 B^2 S e^{Ar^2}\left(3\alpha - 2\beta r^2\right) \\ &+ 16A^4 B^4 S^2 r^2 e^{2Ar^2}\left(-2\alpha + \beta r^2\right)\Big] \Big/ \\ &\Big[4\pi(3m-1)\left(1 + 4A^2 B^2 S r^2 e^{Ar^2}\right)^2\Big],\end{aligned} \tag{37}$$

$$\begin{aligned}P_r = m\Big[&16\pi B_g\left(1 + 4A^2 B^2 S r^2 e^{Ar^2}\right)^2 + 3\alpha A \\ &+ 8\alpha A^3 B^2 S r^2 e^{Ar^2} + \beta - 4A^2 B^2 S e^{Ar^2}\left(3\alpha - 2\beta r^2\right) \\ &+ 16A^4 B^4 S^2 r^2 e^{2Ar^2}\left(-2\alpha + \beta r^2\right)\Big] \Big/ \\ &\Big[4\pi(3m-1)\left(1 + 4A^2 B^2 S r^2 e^{Ar^2}\right)^2\Big],\end{aligned} \tag{38}$$

$$\begin{aligned}P_t = &\Big[32\pi m B_g\left(1 + 4A^2 B^2 S r^2 e^{Ar^2}\right)^2 + 6\alpha m A \\ &- 8\alpha A^3 B^2 S(m-1) r^2 e^{Ar^2} + 2m\beta + 16A^4 B^4 S^2 r^2 e^{2Ar^2} \\ &\times\left(-\alpha(1+m) + 2\beta m r^2\right) + A^2\left(-24\alpha m S B^2 e^{Ar^2}\right. \\ &\left. + r^2\left(-\alpha + 3m\alpha + 16\beta m S B^2 e^{Ar^2}\right)\right)\Big] \Big/ \\ &\Big[4\pi(3m-1)\left(1 + 4A^2 B^2 S r^2 e^{Ar^2}\right)^2\Big].\end{aligned} \tag{39}$$

The values of density and pressure due to quark matter read

$$\begin{aligned}\sigma^q = &\Big[-64\pi B_g\left(1 + 4A^2 B^2 S r^2 e^{Ar^2}\right)^2 \\ &+ 3\left(-4\alpha A + 16\alpha A^3 B^2 S(m-1) r^2 e^{Ar^2} - (1+m)\beta\right. \\ &- 16\alpha A^4 B^4 S^2 r^2 e^{2Ar^2} \\ &\times (1+m)(-2\alpha + \beta r^2) + 8A^2 B^2 S e^{Ar^2} \\ &\left.\left(\alpha + 3m\alpha - (1+m)\beta r^2\right)\right)\Big] \Big/ \\ &\Big[16\pi(3m-1)\left(1 + 4A^2 B^2 S r^2 e^{Ar^2}\right)^2\Big],\end{aligned} \tag{40}$$

$$\begin{aligned}P^q = &\Big[-64\pi m B_g\left(1 + 4A^2 B^2 S r^2 e^{Ar^2}\right)^2 \\ &- 4\alpha A + 16\alpha A^3 B^2 S(m-1) r^2 e^{Ar^2} - (1+m)\beta \\ &- 16\alpha A^4 B^4 S^2 r^2 e^{2Ar^2} \\ &\times (1+m)(-2\alpha + \beta r^2) + 8A^2 B^2 S e^{Ar^2} \\ &\left(\alpha + 3m\alpha - (1+m)\beta r^2\right)\Big] \Big/ \\ &\Big[16\pi(3m-1)\left(1 + 4A^2 B^2 S r^2 e^{Ar^2}\right)^2\Big].\end{aligned} \tag{41}$$

The anisotropy arising form the normal content of the hybrid self-gravitating star is defined as

$$\Delta \equiv P_t - P_r = \frac{\alpha A^2\left(1 - 4AS B^2 e^{Ar^2}\right) r^2}{8\pi\left(1 + 4A^2 B^2 S r^2 e^{Ar^2}\right)^2}, \tag{42}$$

and $\frac{2\Delta}{r}$ corresponds to the anisotropic force, exhibiting a repulsive nature for $\Delta < 0$ and an attractive nature for $\Delta > 0$. Figure 3 depicts the variation of the anisotropy Δ. It is apparent from the figure that $\Delta > 0$, meaning $P_t > P_r$, which confirms that anisotropic force is repulsive. Furthermore, $\Delta \to 0$ as $r \to 0$, implying that Δ vanishes at the core of the hybrid composition, an expected feature of a viable stellar system.

The central values of the matter density and stress components are defined as

$$\sigma(0) = \frac{16\pi B_g + 3\alpha A + \beta - 12\alpha S A^2 B^2}{4\pi(1 - 3m)}, \tag{43}$$

Table 1 The numerical values of A, B, S, and B_g for different self-gravitating pulsars by taking $m = 0.4$

Compact Star	$M(M_\odot)$	R(km)	A (km^{-2})	B	S (km^{-2})	B_g (km^{-2})
(S1) SAX J1804.4-3658 (SS1)	1.435	7.07	0.0068354	−0.649715	0.0123134	0.000806253
(S2) EXO1745-248	1.4	11	0.00141101	−0.792751	0.0475357	0.000798647
(S3) 4U1820-30	1.58	9.1	0.00321209	−0.707315	0.0238472	0.000801307
(S4) 4U1608-52	1.74	9.3	0.00345669	−0.681239	0.0231137	0.000801425
(S5) PSR J0740+6620	2.072	12.39	0.00163683	−0.719487	0.045898	0.000798663
(S6) PSR J0030+0451	1.44	13.02	0.000837727	−0.822008	0.0766373	0.000797578
(S7) Cen X-4	1.57	9.308	0.00293794	−0.716756	0.0256826	0.000800931
(S8) SAX J1804.4-3658 (SS2)	1.3238	6.35	0.0088673	−0.638577	0.0967094	0.000809059

$$P_r(0) = P_t(0) = \frac{m\left(16\pi B_g + 3\alpha A + \beta - 12\alpha S A^2 B^2\right)}{4\pi(1-3m)}. \tag{44}$$

An analysis of $\sigma(0)$, $P_r(0)$, and $P_t(0)$ reveals that they are finite and positive at the core of the system, ensuring the model's singularity-free nature.

4.1 Boundary conditions in $f(\mathbb{Q})$ gravity

This subsection is devoted to finding the values of the constant parameters in the gravitational potentials through the smooth matching of the inner and outer metrics at the boundary $r = R$, where $r > 2M$ [52]. The Schwarzschild metric serves as the exterior spacetime, defined as

$$ds_+^2 = \left(1 - \frac{2M}{r}\right) dt^2 - \left(1 - \frac{2M}{r}\right)^{-1} dr^2 - r^2\left(d\theta^2 + \sin^2\theta d\phi^2\right). \tag{45}$$

The continuity of the metric potentials g_{tt}, g_{rr}, and $\frac{\partial g_{rr}}{\partial r}$ across the boundary $r = R$, provides

$$\left(1 - \frac{2M}{R}\right) = B^2 e^{Ar^2}, \tag{46}$$

$$\left(1 - \frac{2M}{R}\right)^{-1} = 1 + 4SA^2B^2r^2e^{Ar^2}, \tag{47}$$

$$\frac{M}{R^2} = 2AB^2re^{Ar^2}, \tag{48}$$

However, we use the condition $P_r(R) = 0$ to determine the value of the constant B_g as

$$B_g = \frac{\left[-3\alpha A + \left(12\alpha SA^2B^2 - 8\alpha SA^3B^2R^2 - 8\beta SA^2B^2R^2\right)e^{AR^2} + \left(32\alpha S^2R^2A^4B^4 - 16\beta S^2A^4B^4R^4\right)e^{2AR^2}\right]}{16\pi\left(1 + 4A^2B^2R^2Se^{Ar^2}\right)^2}. \tag{49}$$

The numerical values of B_g subject to different self-gravitating pulsar models are given in Table 1. Now, solving the set of Eqs. (46)–(48), we have

$$A = -\frac{M}{(2M-R)R}, \tag{50}$$

$$B = -\frac{\sqrt{M}e^{-\frac{AR^2}{2}}}{\sqrt{A}R^{3/2}}, \tag{51}$$

$$S = \frac{R}{2A(R-2M)}. \tag{52}$$

Using the mathematical formulations mentioned above, we can obtain numerical values for the model parameters describing well-known self-gravitating pulsars. Table 1 provides a few examples of these dense-matter compact objects.

5 Structural features

The physical validity of any dense-matter, non-rotating spherical configuration, such as ultra-compact self-gravitating systems, black holes, neutron stars, and hybrid matter configurations, depends on the consistent behavior of their physical and geometric variables associated with the system. In this context, the relativistic matter must satisfy the following astrophysical constraints.

1. The geometric functions $e^{a(r)}$ and $e^{b(r)}$, corresponding to the relativistic strange-matter configuration, should align with standard criteria. Specifically, they should be monotonically increasing and positive throughout.
2. The structural variables, including matter density and stress components associated with the relativistic matter,

should remain non-negative throughout the dense matter, i.e., $\sigma, P_r, P_t > 0$ for $0 \leq r < R$. Additionally, P_r should be zero at the boundary of the hybrid star, i.e., $P_r(r = R) = 0$.
3. The r-derivatives of structural variables should be negative, i.e., $\frac{\partial \sigma}{\partial r} < 0$, $\frac{\partial P_r}{\partial r} < 0$, and $\frac{\partial P_t}{\partial r} < 0$. The structural variables should be maximum at the core and exhibit a gradually decreasing trend toward the boundary.
4. The gravitational anisotropy (Δ), which arises due to the decomposition stress components, must be zero at the center because $P_r = P_t$ at the center of the gravitational configuration.

The profiles of $e^{a(r)}, e^{b(r)}, \sigma, P_r, P_t, \frac{\partial \sigma}{\partial r}, \frac{\partial P_r}{\partial r}$, and $\frac{\partial P_t}{\partial r}$ for the assumed self-gravitating compact star models are displayed in Figs. 1, 2, 3, 4 and 5. Their profiles demonstrate that the presented solution for the hybrid self-gravitating star model satisfies the requirements outlined in 1–4.

5.1 Energy criteria

Matter distribution in dense stars, particularly in GR and extended models, depends critically on energy conditions. These conditions reflect the fundamental physical laws and provide an effective framework for determining the realistic behavior of astrophysical formations. Generally, energy conditions are divided into four categories, with the following mathematical representations

$$\text{(i)Weak Energy Conditions (WEC)} : \sigma + P_r \geq 0, \quad \sigma + P_t \geq 0, \tag{53}$$

$$\text{(ii)Null Energy Conditions (NEC)} : \sigma \geq 0, \quad \sigma + P_r \geq 0, \ \sigma + P_t \geq 0, \tag{54}$$

$$\text{(ii)Dominant Energy Conditions (DEC)} : \sigma \geq |P_r|, \quad \rho \geq |P_t|, \tag{55}$$

$$\text{(iii)Strong Energy Conditions (SEC)} : \sigma + P_r + 2P_t \geq 0, \quad \sigma + P_r \geq 0, \ \sigma + P_t \geq 0. \tag{56}$$

These inequalities are necessary conditions for the viability of any realistic astrophysical fluid sphere with an anisotropic fluid distribution. All energy conditions in our analysis exhibit stable and positive behavior throughout the stellar interior, as shown in Fig. 6 for the considered self-gravitating pulsar models.

5.2 Stability analysis of the proposed model

To understand the realistic nature of gravitationally confined stellar formations, it is essential to fulfill certain astrophysical constraints. These constraints act as critical criteria to ensure the stability and viability of the proposed self-gravitating star solution. The construction of these constraints is as follows.

5.2.1 Hydrostatic equilibrium condition in $f(\mathbb{Q})$ gravity

For a dense-matter relativistic sphere to be realistic, it must be in hydrostatic equilibrium. We employ the generic form of the TOV equation within the linear $f(\mathbb{Q})$ model to ensure the hydrostatic equilibrium of the proposed compact star candidate. This is characterized by the following mathematical expression

$$\frac{2}{r}(P_t - P_r) - \frac{\partial P_r}{\partial r} - \frac{a'}{2}(\sigma + P_r) - \frac{a'}{2}\left(\sigma^q + P_r^q\right) - \frac{\partial P^q}{\partial r} = 0, \tag{57}$$

which can be alternatively defined as

$$F_h + F_g + F_a + F_q = 0, \tag{58}$$

where

$$F_a = \frac{2}{r}(P_t - P_r), \tag{59}$$

$$F_h = -\frac{dP_r}{dr}, \tag{60}$$

$$F_g = -\frac{a'}{2}(\sigma + P_r), \tag{61}$$

$$F_q = -\frac{a'}{2}\left(\sigma^q + P_r^q\right) - \frac{dP^q}{dr}, \tag{62}$$

denote the anisotropic force, hydrostatic force, gravitational force, and quark matter force, respectively. Figures 7, 8, 9 and 10 describe the profiles of the F_a, F_h, F_g, and F_q subject to the self-gravitating hybrid star. These profiles illustrate that all the forces counterbalance each other, resulting in a state of static equilibrium for the suggested stellar model.

5.2.2 Adiabatic perturbations

The adiabatic index is significant parameter for understanding the robustness of self-gravitating stellar formations like hybrid stars or neutron stars [83]. This explains the relationship between density and pressure in an adiabatic process. The mathematical representation of the adiabatic index is defined as

$$\Gamma = \frac{\sigma + P}{P}\frac{\partial P}{\partial \sigma}. \tag{63}$$

Since $P_r \neq P_t$, for an anisotropic stellar configuration, therefore the modified form of Γ becomes a function of both P_r

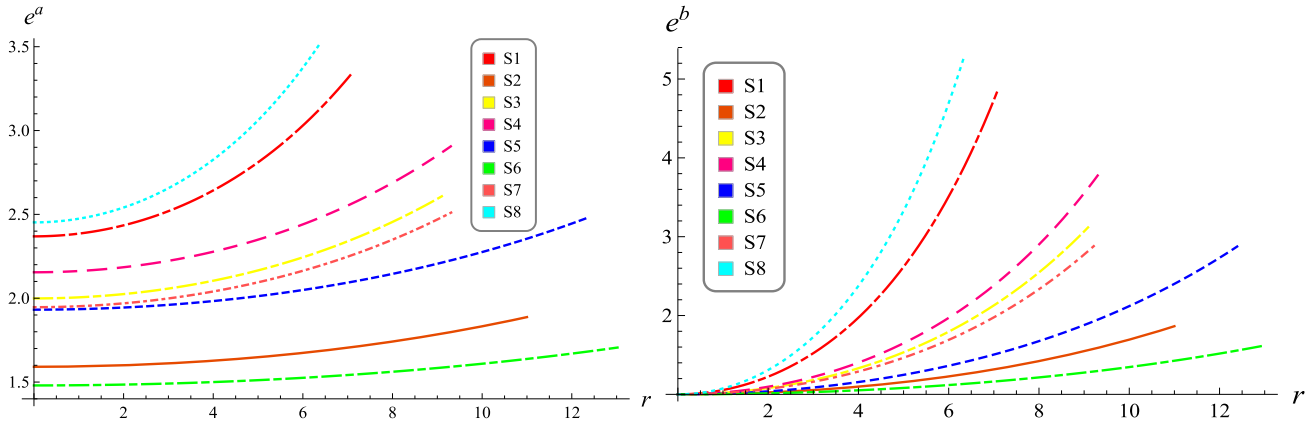

Fig. 1 Plots of gravitational potentials against r

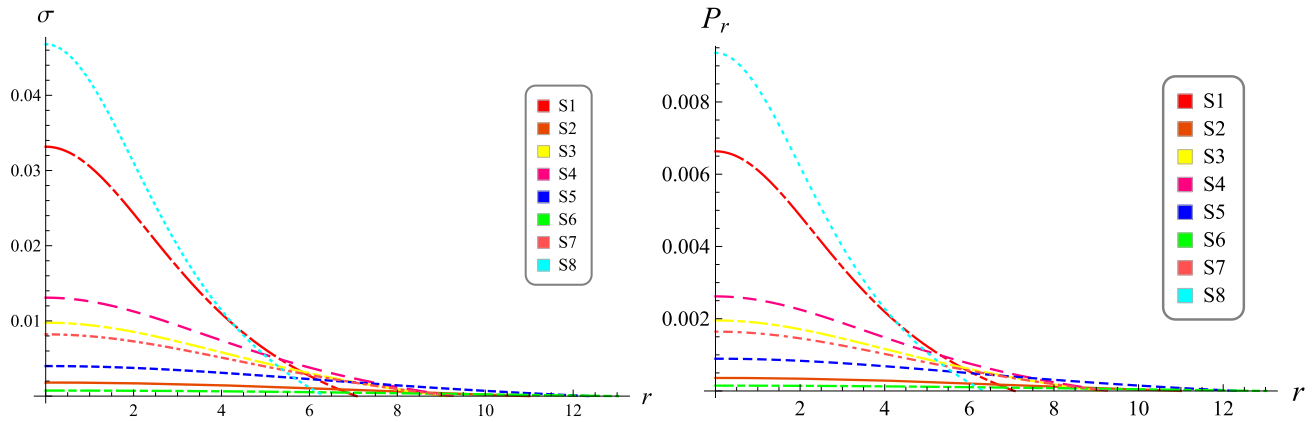

Fig. 2 Behaviors of σ and P_r against r

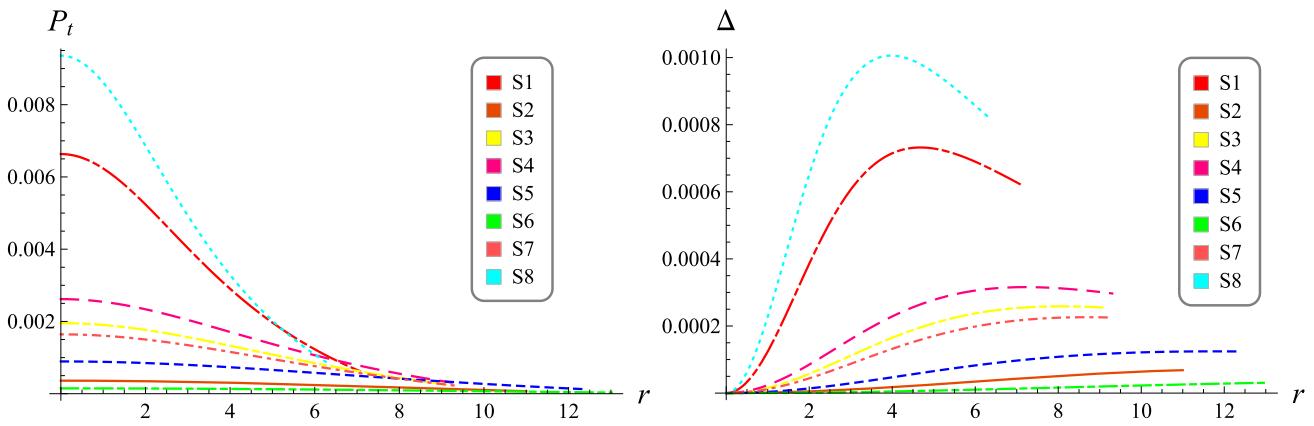

Fig. 3 Plots of P_t and Π against r for the considered self-gravitating pulsars

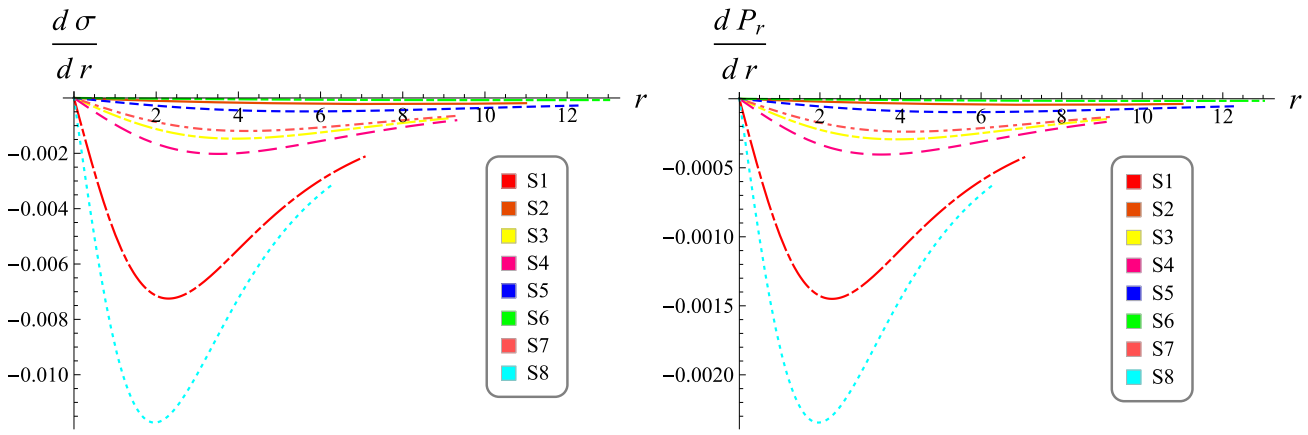

Fig. 4 Plots of σ-gradient and P_r-gradient against r

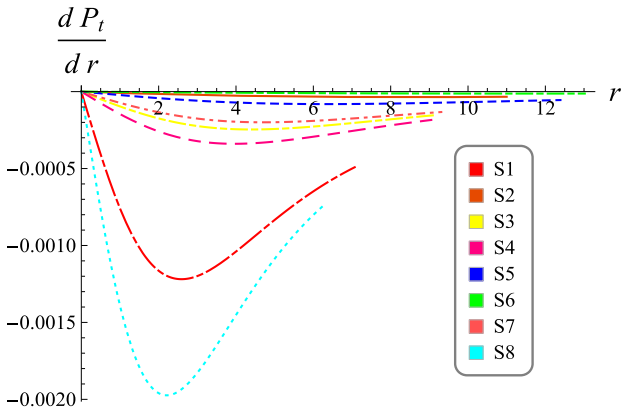

Fig. 5 Plot of P_t-gradient versus r

and P_t. Thus, the expression for the adiabatic index in such a case is modified as

$$\Gamma_r = \left(\frac{\sigma + P_r}{P_r}\right)\frac{\partial P_r}{\partial \sigma} \quad \text{and} \quad \Gamma_t = \left(\frac{\sigma + P_t}{P_t}\right)\frac{\partial P_t}{\partial \sigma}. \tag{64}$$

Bondi [84] established the stability criterion for a self-gravitating sphere: stability requires $\Gamma > 4/3$, while $\Gamma = 4/3$ corresponds to a state of neutral equilibrium. Figure 11 shows the the variations of radial tangential adiabatic indices (Γ_r and Γ_t) against r for different self-gravitating pulsar models. We observe that both Γ_r and Γ_t are greater than $4/3$ throughout the self-gravitating configuration, which ensures the stability of the suggested stellar model against adiabatic perturbations.

5.2.3 Herrera's cracking method

Among the essential physical conditions for ensuring the validity of the proposed relativistic solution, causality holds the utmost importance. According to this criterion, the radial (V_r^2) and tangential (V_t^2) components of sound velocity should be less than 1. Mathematically, these components are defined as

$$V_r^2 = \frac{\partial P_r}{\partial \rho} = m, \tag{65}$$

$$V_t^2 = \frac{\partial P_t}{\partial \rho}. \tag{66}$$

The graphs for the velocity components V_r^2 and V_t^2 for the proposed anisotropic spherical fluid sphere model corresponding to the considered compact stars are presented in Fig. 12. The Figure makes it evident that $0 < V_r^2 \leq 1$ and $0 < V_t^2 \leq 1$ throughout the stellar formation. The stability of self-gravitating structures, particularly in the case of stellar configurations, is investigated using Herrera's stability criteria, based on the analysis of radial and tangential sound speeds. According to this criterion, known as the 'cracking method,' a model may be stable if the transverse pressure wave speed is greater than the radial pressure wave speed, i.e., $V_t^2 - V_r^2 < 0$. Furthermore, since $0 < V_r^2 \leq 1$ and $0 < V_t^2 \leq 1$, the presented solution also satisfies Andreasson's assertion that $|V_t^2 - V_r^2| \leq 1$ (see Fig. 13).

5.2.4 EoS parameters

The EoS parameters are characterized by the matter density ratio to the fluid's pressure within the astrophysical compact matter configuration. The mathematical representations of the EoS parameters for an anisotropic stellar fluid are defined as

$$\omega_r = \frac{P_r}{\sigma}, \quad \omega_t = \frac{P_t}{\sigma} \tag{67}$$

These parameters offer key information regarding the dense-matter configuration of self-gravitating stars. To describe the realistic character of dense matter, the EoS parameters should

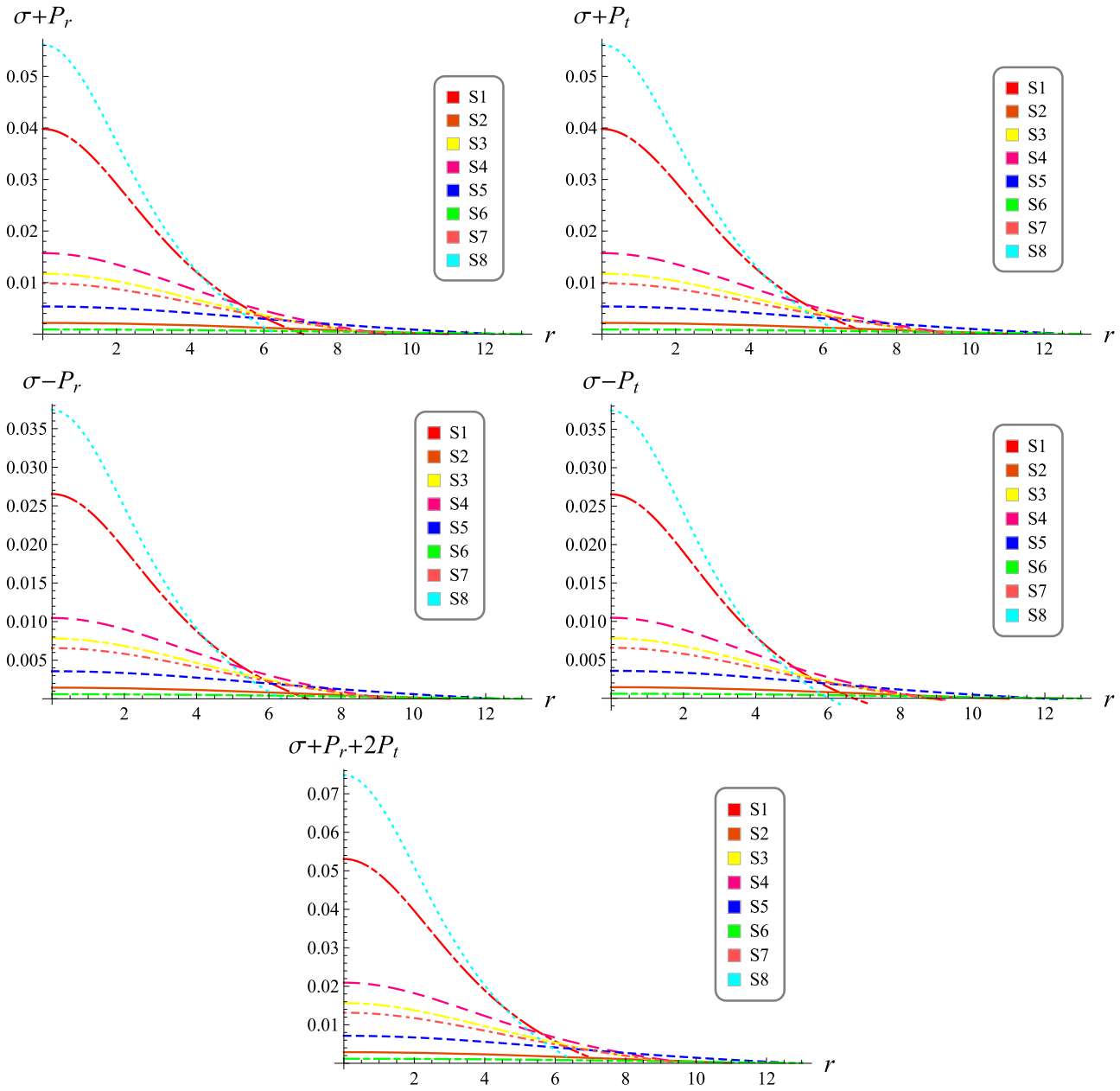

Fig. 6 Plot of energy conditions versus r

satisfy the following constraints

$$0 < \omega_r < 1, \quad 0 < \omega_t < 1, \tag{68}$$

for all the considered self-gravitating pulsar models within the background of the linear functional form of $f(\mathbb{Q})$ gravity. The graphical analysis describing the radial and tangential fluctuations of the EoS parameters ω_r and ω_t is presented in Fig. 14. Their profiles illustrate that ω_r and ω_t satisfy the constraint (68). These results imply that the EoS parameter fluctuations associated with the proposed hybrid star model are consistent with astrophysical constraints.

6 Additional characteristics associated with hybrid configuration

6.1 Effective mass function

A mathematical tool used to characterize the overall gravitational mass contained within a dense-matter spherical configuration is calculated using the Misner-Sharp criterion. This criterion has the following mathematical form

$$M(r) = \frac{r}{2}\left(1 - g^{\mu\nu}\partial_\mu r \partial_\nu r\right), \tag{69}$$

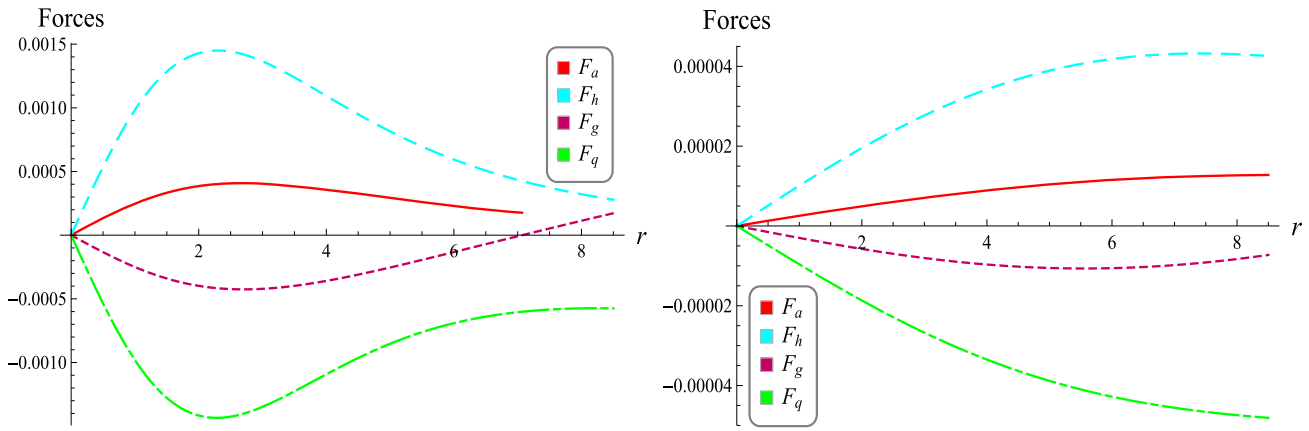

Fig. 7 Graphical illustration of all forces for the compact star S1 (left panel) and S2 (right panel) versus r

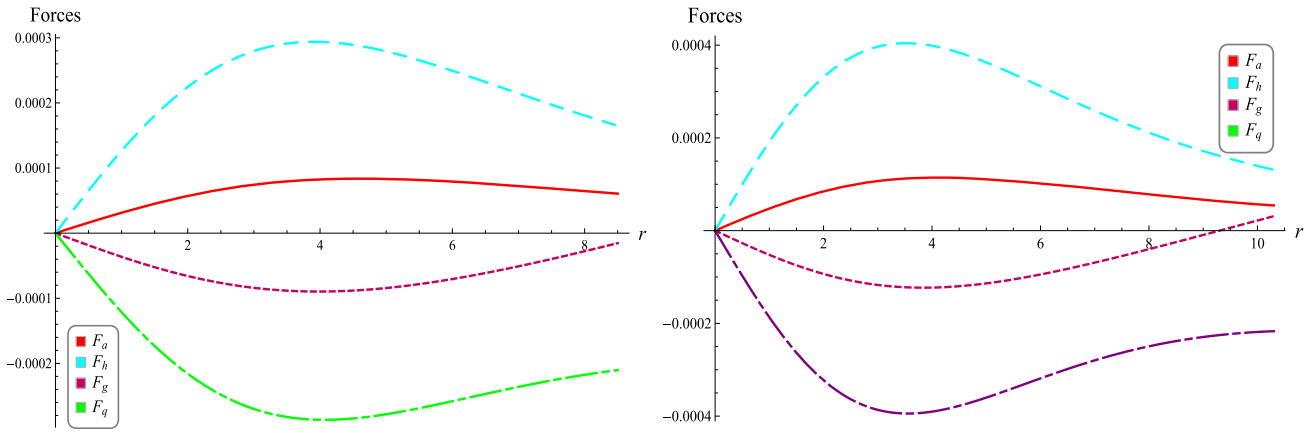

Fig. 8 Behavior of all forces for the self-gravitating pulsars S3 (left panel) and S4 (right panel) versus r

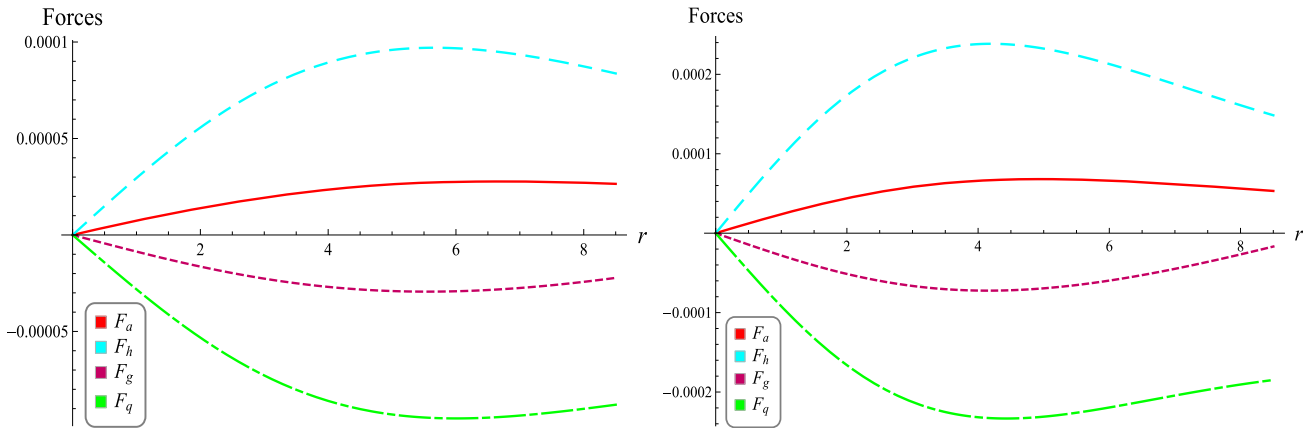

Fig. 9 Graphical analysis of all forces for the stellar configurations S5 (left panel) and S6 (right panel) versus r

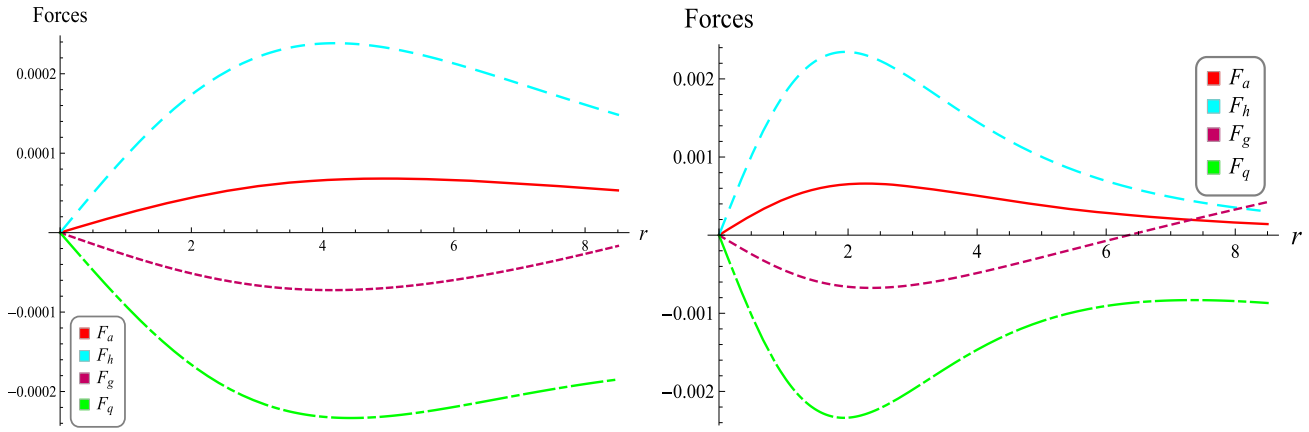

Fig. 10 Behavior of all forces for the compact stars S7 (left panel) and S8 (right panel) versus r

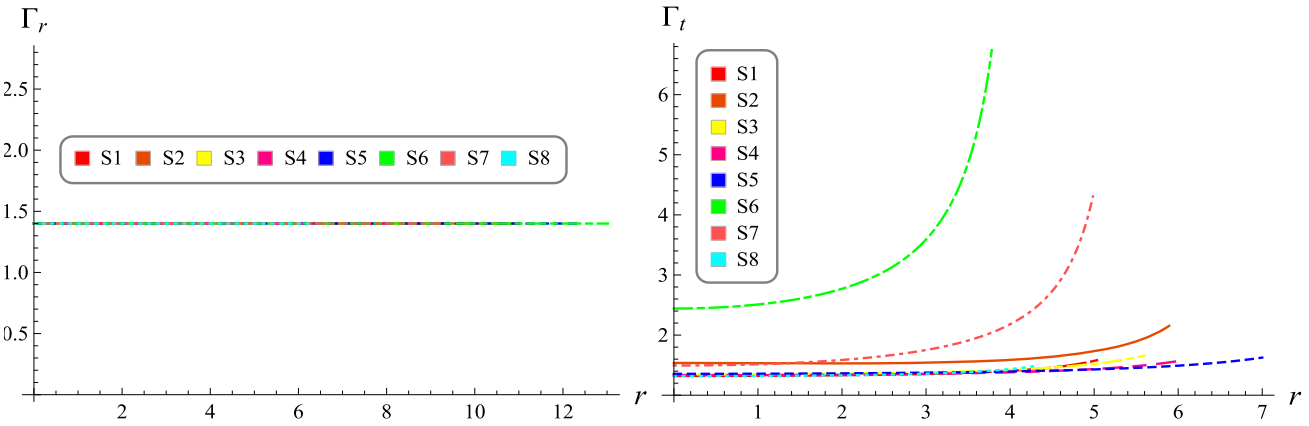

Fig. 11 Variations of Γ_r and Γ_t against r

15

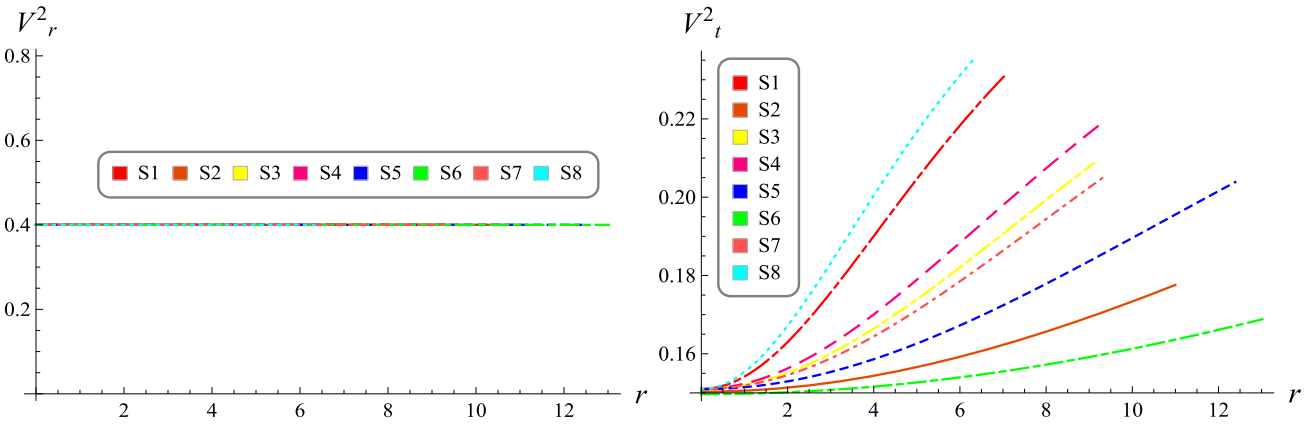

Fig. 12 Behaviors of V_r^2 (left panel) and V_t^2 (right panel) against r

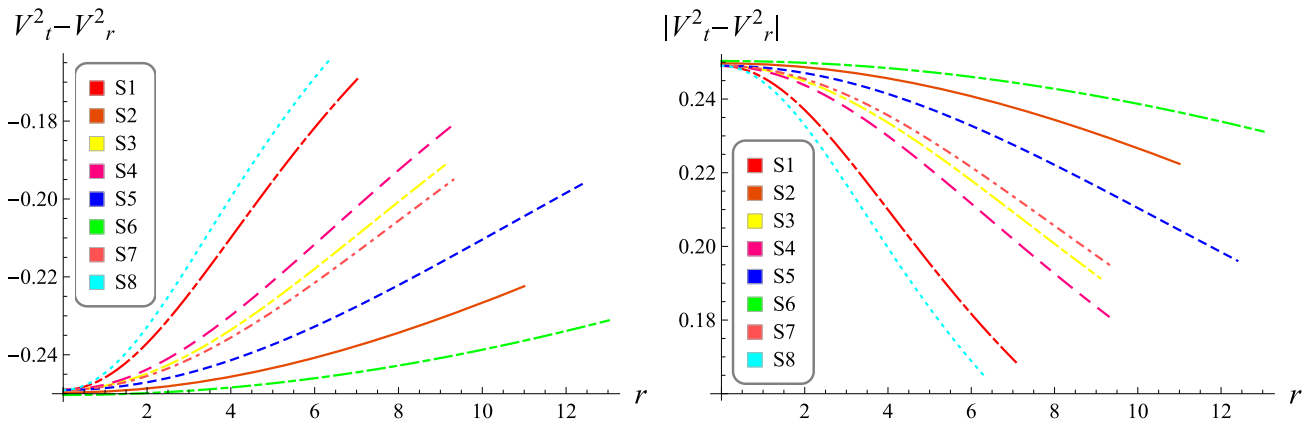

Fig. 13 Variations of $V_t^2 - V_r^2$ (left panel) and $|V_t^2 - V_r^2|$ (right panel) against r

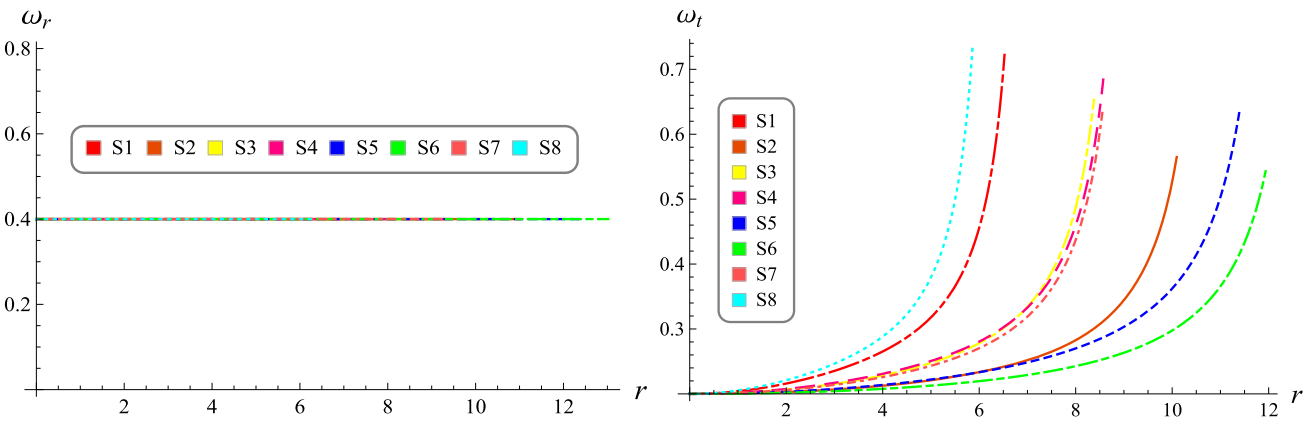

Fig. 14 Variations of ω_r (left panel) and ω_t (right panel) against r

which gives

$$M(r) = \frac{r}{2}\left(1 - e^{-b(r)}\right), \tag{70}$$

or, equivalently as

$$M(r) = 4\pi \int_0^r r^2 \sigma(x) dx, \tag{71}$$

Therefore, the expression of effective mass for the considered anisotropic configuration can be given by

$$\begin{aligned} M(r)^{eff} &= 4\pi \int_0^r r^2 \sigma^{eff}(x) dx \\ &= 4\pi \int_0^r r^2 \left(\sigma + \sigma^q\right)(x) dx. \end{aligned} \tag{72}$$

The behavior of M^{eff} against r for the considered compact stars is shown in Fig. 15. The graphical examination shows that M^{eff} is a positive and gradually increasing function of r throughout the self-gravitating stellar structure. The viable behavior of the mass function ensures the physical viability of the presented relativistic solution.

6.2 Compactness

The compactness of the self-gravitating dense-matter configuration is determined by a dimensionless parameter, defined as

$$U^{eff} = \frac{M^{eff}}{r} \tag{73}$$

Figure 16 illustrates the graphical representation of U^{eff}, showing a monotonically increasing trend with respect r.

6.3 Effective surface redshift

The effective surface redshift, denoted as Z_s^{eff}, for the current stellar formation, can be determined by employing the expression of the effective compactness factor, U^{eff}, as fol-

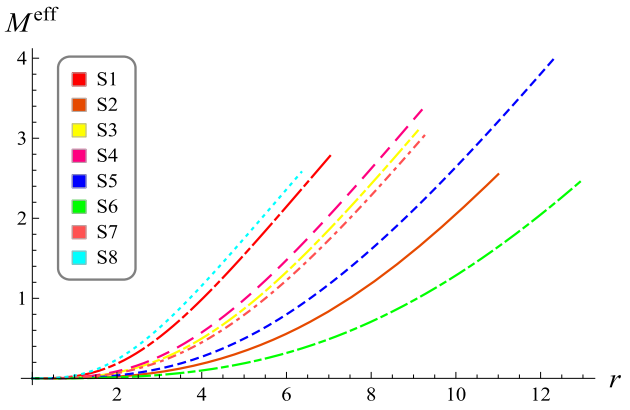

Fig. 15 Plot of M^{eff} against r

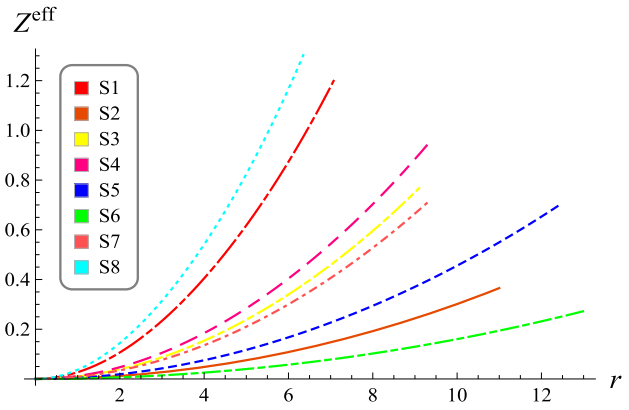

Fig. 17 Plot of Z^{eff} versus r

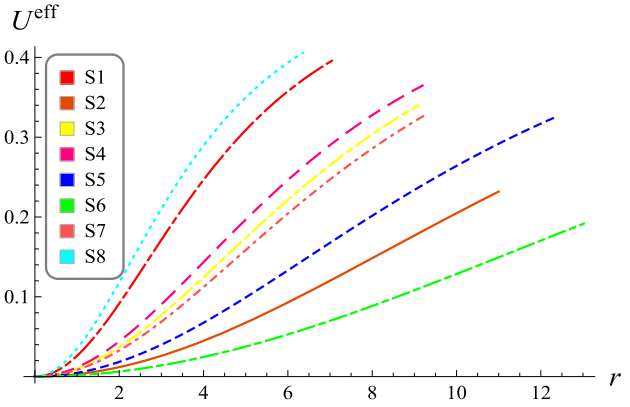

Fig. 16 Variation of U^{eff} versus r

lows

$$Z_s^{eff} = \frac{1}{\sqrt{1-2U^{eff}}} - 1. \tag{74}$$

The graphical analysis of Z_s^{eff}, showing a monotonically increasing trend concerning the radial coordinate r. Ivanov [85] suggests that a self-gravitating, anisotropic formation may reach a maximum surface redshift of 3.842. The profile of Z_s^{eff} shows that the presented stellar model satisfies the Ivanov's limit.

7 Conclusion

According to recent investigations of extremely dense astrophysical configurations, the pressure inside these stellar objects is anisotropic in nature, and their densities are often higher than that of nuclear matter. In this respect, hybrid quark stars have emerged as prominent candidates for understanding the relativistic composition of anisotropic, compact astrophysical objects in recent years. We have successfully modeled an anisotropic hybrid compact star whose matter distribution consists of two components: normal matter and quark matter. The distribution of quark matter is modeled by assuming the widely known MIT bag model EoS. The proposed model of the hybrid compact configuration is non-singular, spherically symmetric, and non-isotropic in nature. The embedding Class One formalism is used to derive an important correspondence between the radial and temporal gravitational potentials and to simplify the methodology for constructing solutions to the $f(\mathbb{Q})$-field equations. In this investigation, we employed the TK ansatz for the temporal geometric variable, while the radial geometric function was formulated using the embedding Class One condition. The key findings are outlined below:

- The graphical analysis of the gravitational potentials is presented in Fig. 1, which demonstrates that they meet all the necessary requirements and are finite, positive, and free of singularities. Furthermore, the values of the gravitational potentials at the center of the hybrid stellar structure are $ea = B^2$ and $e^b = 1$. Both metric variables exhibit monotonic growth and attain their maximum values near the stellar boundary.
- Figures 2 and 3 display the graphical analysis of the physical variables, such as σ, P_r, and P_t, associated with the Karmarkar-connected hybrid star. The matter density is positive, finite, and a monotonically decreasing function of r. Both stress components gradually decrease from the center toward the boundary of the hybrid composition and attain their maximum values at the core. Furthermore, the radial pressure vanishes at the boundary, i.e., $P_R = 0$. This behavior of the physical variables indicates that the relativistic configuration has a consistent and physically acceptable.
- The graphical analysis of gravitational anisotropy is presented in Fig. 3, which shows that the anisotropy force exhibits a repulsive character. The repulsive nature of the

anisotropic force supports the existence of a viable astrophysical configuration.

- As illustrated in Fig. 7, the graphical analysis of the energy conditions confirms that all energy bounds are satisfied for the considered models of self-gravitating pulsars.
- We investigated the cumulative impact of various external forces, namely F_a, F_h, F_g, and F_q, on the Karmarkar-connected hybrid stellar configuration. It is noted that all these forces are in equilibrium for the considered self-gravitating pulsar objects, which further strengthens the robustness of the proposed anisotropic gravitational solution.
- Figure 11 displays the stability of the Karmarkar-connected hybrid solution against adiabatic perturbations. The profiles of the radial and tangential indices indicate that the compact system is stable in all interior regions.
- Another interesting technique that we have presented to assess the consistency of the compact system is Herrera's cracking criterion displayed in Fig. 13. This characteristic demonstrates that $V_r^2 - V_t^2 < 0$, proving the physical dependability of our model and its suitability for constructing a stable structure.
- The graphical analysis of EoS parameters, ω_r and ω_t, is displayed in Fig. 14. The profiles indicate that $0 < \omega_r < 1$ and $0 < \omega_t < 1$ throughout, confirming the realistic nature of the model.
- Figures 15, 16, and 17 illustrate the behavior of the effective mass, compactness, and redshift. These parameters are observed to increase monotonically with increasing r throughout the stellar interior and lie within the astrophysical constraints.

To summarize, the present work demonstrates the construction of a stable and singularity-free hybrid self-gravitating stellar system. Establishing a link between such dense-matter structures and dark matter could be a fascinating avenue for future research. Such a study could provide new insights into the interaction of matter configurations with the dark sector, possibly advancing our understanding of compact star systems in the context of extended gravitational models. We have found several interesting astrophysical studies related to our work. In this regard, the authors of [86] constructed compact star models by considering the MIT bag model within the framework of non-perturbative $f(R)$ gravity. Similarly, Nashed and Capozziello [87] investigated spherically symmetric dense-matter configurations regulated by an anisotropic fluid distribution, adopting a more general model of $f(R)$ gravity. Their results have been validated using observations of the SAX J1748.9-2021 pulsar. Furthermore, some static, anisotropic, and spherically symmetric models that constrain quadratic $f(R)$ gravity using the self-gravitating pulsar J0704+6620 [88], as well as linear models of curvature-matter coupled gravity applied to the pulsar PSR J0740+6620 [89], could also be relevant to our work. The primary difference between the $f(R)$ and $f(\mathbb{Q})$ gravity models is their underlying geometry. The $f(R)$ gravity model alters Einstein's gravity by applying the Ricci scalar, which is related to curvature. In contrast, $f(\mathbb{Q})$ employs non-metricity, a measure of how geometry differs from traditional distance measurements, to provide a curvature-free solution. This leads to novel ways of simulating gravity. For astrophysical configurations, such as compact objects, $f(\mathbb{Q})$ gravity provides easier adjustments to the equations controlling neutron star construction than $f(R)$, possibly leading to differing mass and stability attributes. Modifications in $f(R)$ gravity arise from curvature alterations, whereas deviations in $f(\mathbb{Q})$ gravity result from non-metricity. This fundamental difference leads to distinct field equations and stellar structures, significantly affecting quark star equilibrium. We have demonstrated through our analysis that $f(\mathbb{Q})$ gravity alters both the mass-radius relationship and the stability of quark stars.

Acknowledgements This research has been funded by the Scientific Research Deanship at the University of Haíl, Saudi Arabia through project number: NT-24 013.

Data Availability Statement My manuscript has no associated data. [Authors' comment: All data generated or analyzed during this study are included in this published article.]

Code Availability Statement My manuscript has no associated code/software. [Author's comment: Code/Software sharing not applicable to this article as no code/software was generated or analysed during the current study.]

Declarations

Conflict of interest The authors declare no conflict of interest.

Funded by SCOAP[3].

References

1. V.A. Dexheimer, S. Schramm, Phys. Rev. C **81**, 045201 (2010)
2. J.P. Pereira, C.V. Flores, G. Lugones, Astrophys. J. **860**, 12 (2018)

3. C. Maieron, M. Baldo, G.F. Burgio, H.-J. Schulze, Phys. Rev. D **70**, 043010 (2004)
4. S.Y. Lau, K. Yagi, Phys. Rev. D **103**, 063015 (2021)
5. L. Bonanno, A. Sedrakian, Astron. Astrophys. **539**, A16 (2012)
6. S.M. Carroll, V. Duvvuri, M. Trodden, M.S. Turner, Phys. Rev. D **70**, 043528 (2004)
7. R.R. Caldwell, M. Kamionkowski, Annu. Rev. Nucl. Part. Sci. **59**, 397 (2009)
8. Z. Yousaf, Phys. Dark Universe (2025) (**To appear**)
9. A.G. Riess et al., Astron. J. **116**, 1009 (1998)
10. A.G. Riess et al., Astrophys. J. **607**, 665 (2004)
11. D.N. Spergel et al., Astrophys. J. Suppl. Ser. **148**, 175 (2003)
12. S. Capozziello, A. Stabile, A. Troisi, Phys. Rev. D **76**, 104019 (2007)
13. S. Capozziello, V.F. Cardone, V. Salzano, Phys. Rev. D **78**, 063504 (2008)
14. N. Katırcı, M. Kavuk, Eur. Phys. J. Plus **129**, 163 (2014)
15. M.F. Shamir, M. Ahmad, Phys. Rev. D **97**, 104031 (2018)
16. I. de Martino, M. De Laurentis, S. Capozziello, Phys. Rev. D **102**, 063508 (2020)
17. M. Bhatti, Z. Yousaf, S. Khan, Int. J. Mod. Phys. D **30**, 2150097 (2021)
18. S.-W. Wei, Y.-X. Liu, Eur. Phys. J. Plus **136**, 436 (2021)
19. M.Z. Bhatti, M.Y. Khlopov, Z. Yousaf, S. Khan, Mon. Not. R. Astron. Soc. **506**, 4543 (2021)
20. F. Canfora, A. Cisterna, S. Fuenzalida, C. Henríquez-Báez, J. Oliva, Phys. Rev. D **104**, 044026 (2021)
21. M.Z. Bhatti, Z. Yousaf, Z. Tariq, Chin. J. Phys. **72**, 18 (2021)
22. Z. Yousaf, M.Z. Bhatti, S. Khan, Int. J. Mod. Phys. D **31**, 2250099 (2022)
23. Z. Yousaf, M.Z. Bhatti, S. Khan, Ann. Phys. **534**, 2200252 (2022)
24. M.Z. Bhatti, Z. Yousaf, S. Khan, Chin. J. Phys. **77**, 2168 (2022)
25. E. Battista, V. De Falco, Eur. Phys. J. C **82**, 628 (2022)
26. E. Battista, H.C. Steinacker, Eur. Phys. J. C **82**, 909 (2022)
27. V. De Falco, E. Battista, Phys. Rev. D **108**, 064032 (2023)
28. Z. Yousaf, Phys. Scr. **97**, 025301 (2022)
29. E. Battista, Phys. Rev. D **109**, 026004 (2024)
30. S. Capozziello, S. De Bianchi, E. Battista, Phys. Rev. D **109**, 104060 (2024)
31. S. Nojiri, S.D. Odintsov, Phys. Rep. **505**, 59 (2011)
32. T. Clifton, P.G. Ferreira, A. Padilla, C. Skordis, Phys. Rep. **513**, 1 (2012)
33. A. Joyce, B. Jain, J. Khoury, M. Trodden, Phys. Rep. **568**, 1 (2015)
34. S. Nojiri, S.D. Odintsov, V.K. Oikonomou, Phys. Rep. **692**, 1 (2017)
35. B. Li, T.P. Sotiriou, J.D. Barrow, Phys. Rev. D Part. Fields Gravit. Cosmol. **83**, 064035 (2011)
36. P. Wu, H. Yu, Phys. Lett. B **693**, 415 (2010)
37. P. Wu, H. Yu, Phys. Lett. B **692**, 176 (2010)
38. K.F. Dialektopoulos, T.S. Koivisto, S. Capozziello, Eur. Phys. J. C **79**, 606 (2019)
39. J.B. Jiménez, L. Heisenberg, T. Koivisto, S. Pekar, Phys. Rev. D **101**, 103507 (2020)
40. J. Lu, X. Zhao, G. Chee, Eur. Phys. J. l C **79**, 530 (2019)
41. O. Sokoliuk, S. Arora, S. Praharaj, A. Baransky, P.K. Sahoo, Mon. Not. R. Astron. Soc. **522**, 252 (2023)
42. M. Milgrom, Phys. Rev. D **100**, 084039 (2019)
43. F. D'Ambrosio, M. Garg, L. Heisenberg, Phys. Lett. B **811**, 135970 (2020)
44. F. Bajardi, D. Vernieri, S. Capozziello, Eur. Phys. J. Plus **135**, 912 (2020)
45. A.S. Agrawal, L. Pati, S.K. Tripathy, B. Mishra, Phys. Dark Universe **33**, 100863 (2021)
46. G.N. Gadbail, A. Kolhatkar, S. Mandal, P.K. Sahoo, Eur. Phys. J. C **83**, 595 (2023)
47. N. Dimakis, A. Paliathanasis, T. Christodoulakis, Class. Quantum Gravity **38**, 225003 (2021)
48. F. Bajardi, S. Capozziello, Eur. Phys. J. C **83**, 531 (2023)
49. W. Wang, H. Chen, T. Katsuragawa, Phys. Rev. D **105**, 024060 (2022)
50. R.-H. Lin, X.-H. Zhai, Phys. Rev. D **103**, 124001 (2021)
51. P. Bhar, Fortschr. Phys. **71**, 2300074 (2023)
52. P. Bhar, J.M.Z. Pretel, Phys. Dark Universe **42**, 101322 (2023)
53. P. Bhar, F. Rahaman, Eur. Phys. J. C **75**, 41 (2015)
54. S.K. Maurya, A. Ashraf, F. Al Khayari, G. Mustafa, M.K. Jasim, Eur. Phys. J. C **84**, 986 (2024)
55. L. Herrera, N.O. Santos, Phys. Rep. **286**, 53 (1997)
56. Z. Yousaf, B. Almutairi, S. Khan, and K. Bamba, Phys. Dark Universe p. 101727 (2024)
57. S. Khan, Z. Yousaf, Phys. Scr. **99**, 055303 (2024)
58. A.M. Albalahi, M. Bhatti, A. Ali, S. Khan, Eur. Phys. J. C **84**, 293 (2024)
59. A.M. Albalahi, Z. Yousaf, S. Khan, A. Ali, Eur. Phys. J. C **84**, 963 (2024)
60. Z. Yousaf, T. Ganesan, B. Almutairi, M.Z. Bhatti, S. Khan, Phys. Scr. **99**, 125302 (2024)
61. S. Khan, A. Adeel, Z. Yousaf, Eur. Phys. J. C **84**, 572 (2024)
62. A. Malik, M. Aslam, S. Chaudhary, A. Almas, G. K, Ann. Phys. 169896 (2024)
63. Z. Yousaf, K. Bamba, B. Almutairi, S. Khan, M. Bhatti, Class. Quantum Gravity **41**, 175001 (2024)
64. S. Khan, Z. Yousaf, Phys. Scr. **99**, 095304 (2024)
65. R.F. Sawyer, Phys. Rev. Lett. **29**, 382 (1972)
66. R. Ruffini, S. Bonazzola, Phys. Rev. **187**, 1767 (1969)
67. M. Gleiser, Phys. Rev. D **38**, 2376 (1988)
68. J.H. Jeans, Mon. Not. R. Astron. Soc. **82**, 122 (1922)
69. M. Ruderman, Ann. Rev. Astron. Astrophys. **10**, 427 (1972)
70. W. Hillebrandt, K.O. Steinmetz, Astron. Astrophys. **53**, 283 (1976)
71. Z. Yousaf, A. Adeel, S. Khan, M.Z. Bhatti, Chin. J. Phys. **88**, 406 (2023)
72. K.R. Karmarkar, in *Proc. Indian Acad. Sci. A*, vol. 27 (Springer, 1948), p. 56
73. S.N. Pandey, S.P. Sharma, Gen. Relativ. Gravit. **14**, 113 (1982)
74. S.K. Maurya, Y.K. Gupta, B. Dayanandan, S. Ray, Eur. Phys. J. C **76**, 266 (2016)
75. S.K. Maurya, M. Govender, S. Kaur, R. Nag, Eur. Phys. J. C **82**, 100 (2022)
76. P. Bhar, Phys. Dark Universe **34**, 100879 (2021)
77. D. Zhao, Eur. Phys. J. C **82**, 303 (2022)
78. J.B. Jiménez, L. Heisenberg, T. Koivisto, Phys. Rev. D **98**, 044048 (2018)
79. J.B. Jiménez, L. Heisenberg, T.S. Koivisto, J. Cosmol. Astropart. Phys. **2018**, 039 (2018)
80. D. Bao, S.-S. Chern, Z. Shen, An introduction to Riemann-Finsler geometry, vol. 200 (Springer Science & Business Media, 2012)
81. E. Witten, Phys. Rev. D **30**, 272 (1984)
82. K.S. Cheng, Z.G. Dai, T. Lu, Int. J. Mod. Phys. D **7**, 139 (1998)
83. R. Chan, L. Herrera, N.O. Santos, Mon. Not. R. Astron. Soc. **265**, 533 (1993)
84. H. Bondi, Proc. R. Soc. Lond. Ser. A. Math. Phys. Sci. **281**, 39 (1964)
85. B.V. Ivanov, Phys. Rev. D **65**, 104011 (2002)
86. A.V. Astashenok, S. Capozziello, S.D. Odintsov, Phys Lett. B **742**, 160 (2015)
87. G.G.L. Nashed, S. Capozziello, Eur. Phys. J. C **84**, 521 (2024)
88. G.G.L. Nashed, W. El Hanafy, J. Cosmol. Astropart. Phys. **2023**, 038 (2023)
89. G.G.L. Nashed, Eur. Phys. J. C **83**, 698 (2023)